

Diffuse Ionized Gas in the Dwarf Irregular Galaxy DDO 53

A.M. Hidalgo-Gómez

*Escuela Superior de Física y Matemáticas, IPN, U.P. Adolfo López Mateos, Mexico City, Mexico*¹

ABSTRACT

The spectral characteristics throughout the dwarf irregular galaxy DDO 53 are studied. The results are very similar to those for other irregular galaxies: high excitation and low values of the $[\text{S II}]/\text{H}\alpha$ ratio. The most likely ionization source is photon leakage from the classical H II regions, without any other source, although the interstellar medium of the galaxy is quite perturbed. Moreover, the physical conditions throughout the galaxy do not change very much because both the photon leakage percentage and the ionization temperature are very similar. In addition, the determined metal content for two H II regions indicates that DDO 53 is a low-metallicity galaxy.

1. Introduction

Diffuse ionized gas (DIG) is defined as ionized gas with a very low density. It is normally localized outside classical H II regions, in the interarm regions of spiral galaxies (Benvenuti et al. 1976), at high altitude over the Galactic plane (Rand et al. 1990), and in very low density regions inside the Milky Way (Reynolds 1983). The spectral characteristics of this gas (low excitation and high values of the $[\text{N II}]/\text{H}\alpha$ and $[\text{S II}]/\text{H}\alpha$ ratios) indicate the existence of extra sources of ionization besides photoionization, such as shocks and turbulence due to stellar winds and other disturbances of the gas.

Such a gas can also be observed in irregular galaxies, at the outermost parts (Hunter & Gallagher 1992) and in the “inter-H II regions” (e.g. Hidalgo-Gómez 2006). The spectral characteristics of the DIG in the few irregular galaxies studied so far (Hidalgo-Gómez 2005, 2006; Hidalgo-Gómez & Peimbert 2007) indicate that the ionization sources are very different from those in spiral galaxies. The DIG of most of these galaxies can be ionized by photon leakage from the H II regions, although the kinematics of the interstellar medium (ISM) is disturbed in some galaxies (GR 8; Hidalgo-Gómez 2006). Only a few of the galaxies studied so far need an extra source of ionization (e.g. Wolf-Rayet stars for IC 10; Hidalgo-Gómez 2005). Our goal is to study the influence of the perturbations of the interstellar medium on the ionization of the DIG, if any, and whether there is any difference for different metallicities, gas masses, or star formation rates. As irregular galaxies comprise a large range in these properties, a large sample of them is needed.

¹On leave from Instituto de Astronomía-UNAM

DDO 53 is a not-very-well-studied dwarf irregular galaxy of the M81 group, but it has three properties which make it a very good candidate for the study of the DIG. First, it has a high gas content with a total gas mass of $2.45 \times 10^8 M_{\odot}$ (Hunter & Elmegreen 2004) and a star formation rate of $5 \times 10^{-3} M_{\odot} \text{ yr}^{-1}$. Second, it is located at only 3.53 Mpc (Hidalgo-Gómez & Olofsson 1998); therefore, the DIG can be detected easily with medium-size telescopes and not very long integration times. Moreover, the spatial resolution is good enough to study the details of the DIG and differentiate it from the classical H II regions. Finally, H α images of the galaxy (Strobel et al. 1990) indicate the existence of gas in between the classical H II regions.

A description of the observations and the data reduction procedure is given in Section 2. Section 3 presents a brief description of the DIG along the slit positions. The ionization source of the DIG is presented in Section 4, while in Section 5 a brief discussion on the spectral characteristics of the DIG of this galaxy compared with previous galaxies is given, as well as a determination of the metallicity. Finally, conclusions are given in Section 6.

2. Observations and data reduction

The spectra of DDO 53 were obtained on 2002 March 12-14 with the 2.1 m telescope of the Observatorio Astronómico Nacional at San Pedro Mártir. The Boller & Chivens spectrograph was used with a 300 line mm^{-1} grating blazed at 5000 Å. The detector was a SITe3 CCD with $3 \mu\text{m}$ pixels in a 1024×1024 format. The slit length was $5'$ and the width was $170 \mu\text{m}$, subtending $\approx 2''$ on the sky, and yielding a spectral resolution of 7 Å. The pixel scale along the spatial direction was $1.05''$. The full spectral range observed was 3500-6900 Å. During the first two nights, strong wind and cirrus made the conditions not very photometric, while the third night the weather conditions improved, although the seeing was higher. Table 1 shows the log of observations. No correction for differential refraction was performed, as the air masses were, in all cases, smaller than 1.3. The orientation of the slit was east-west with a total of eight slit positions.

The reduction of the data was performed with the MIDAS software package. Bias and sky twilight flat-fields were used for the calibration of the CCD response. Due to the strong differences in the sensitivity of the CCD based on the wavelength, the spectral range was divided into three parts: from 5200 to 6800 Å (red), from 4000 to 5600 Å (green), and from 3500 to 4800 Å (blue). Unfortunately, due to the low efficiency of the spectrograph at the blue end, no spectral lines were detected there, and the blue end was therefore not used in the present investigation. He-Ar lamps were used for the wavelength calibration. In addition, the spectra were corrected for geometric deflections. The spectra were corrected for atmospheric extinction using the San Pedro Mártir tables (Schuster & Parrao 2001). Several standard stars were observed each night in order to perform the flux calibration. The accuracy of the calibration was higher than 5% for all nights. The most difficult task was the sky subtraction, because removing the strong sky lines of the spectra also removes most of the low surface brightness emission. In order not to remove this emission, only a dozen rows at each edge of the image were used in the sky templates for each spectrum,

although the emission from the galaxy covered only the central part of the slit. The number of rows, different for each spectrum, was selected as a compromise between the correctness of the results and the maintenance of a low surface brightness emission. This was done by visual inspection. The main problem is that the intensity of neither He I at $\lambda 5875$ nor [O I] $\lambda 6300\text{\AA}$ can be measured because of the proximity of strong sky lines, but these lines are not very commonly seen at low surface brightness. Moreover, sky subtraction which removed all the sky lines, has been performed for other data sets with similar results to those presented here (see, e.g. Hidalgo-Gómez 2006). In any case, special care was taken in the analysis of this data.

This set of data, fully reduced and calibrated, was divided into a number of spectra, covering five rows each. This value matches the seeing conditions during the observations and corresponds to 90 pc at a distance of 3.53 Mpc (Hidalgo-Gómez & Olofsson 1998). A total of 86 one-dimensional spectra were studied, covering eight slit positions throughout the galaxy. These spectra are referred to as the “1D spectra”.

The next step is to correct these spectra for absorption and extinction. The usual procedure in the absorption correction is to increase the equivalent width of $H\beta$ by 2\AA (e.g. McCall et al. 1985). A more accurate absorption correction is to follow Olofsson (1995), who calculated the absorption equivalent width for each Balmer line using different initial mass functions, metallicities, and ages of the star formation event. All these procedures were optimized for H II regions but not for low surface brightness emission, such as studied here. In order to check whether the absorption corrections proposed could be used in the DIG spectrum, we measured other Balmer lines in the DIG when present, made the correction to them, and checked whether the values obtained matched the theoretical ones. The most easily detected line after $H\alpha$ and $H\beta$ is $H\gamma$. This line is detected in some of the spectra. Following McCall et al’s correction, only one out of nine of the $H\gamma$ intensities matched the theoretical one. The same was true when considering Olofsson’s correction. Therefore, as there were no clear absorption features present in the spectra studied here, we preferred not to perform any absorption correction.

The same discussion can be made for the extinction correction. There are two reasons we decided to perform this correction. First, the wavelength range for most of the line ratios is small enough not to be affected by extinction. Second, one of the goals of the investigation is to study the distribution of the extinction inside the galaxy. This correction was performed using the extinction coefficient, defined as

$$C\beta = \frac{1}{f(\lambda)} \ln \frac{I(H\alpha)/I(H\beta)}{2.86}$$

where 2.86 is the theoretical Balmer decrement at 10,000 K for case B of recombination, $f(\lambda)$ is the Whitford modified extinction law (Savage & Mathis 1979), and $I(H\alpha)/I(H\beta)$ is the observed $H\alpha/H\beta$ ratio. The intensities of the lines $H\beta$, [O III] $\lambda 5007$, $H\alpha$, [N II] $\lambda 6583$, He I $\lambda 6678$, [S II] $\lambda 6716$, and [S II] $\lambda 6731$ were measured when present, as well as the flux in the $H\alpha$ line. All the lines were measured twice, except when the two values differed by more than 50%, normally for low signal-to-noise ratio (S/N) lines. For these, a third measurement with a different continuum level

was obtained in order to find a more reliable value for the intensity. With these lines the ratios $[\text{O III}]/\text{H}\beta$, $[\text{O III}]/\text{H}\alpha$, $[\text{N II}]/\text{H}\alpha$, $\text{He I}/\text{H}\beta$ and $[\text{S II}]/\text{H}\alpha$ were obtained.

Finally, we would like to comment on the uncertainties. Three different sources were considered: the uncertainties in the level of the spectral continuum with respect to the lines, σ_c , those introduced by the reduction procedure, (especially flat-fielding and flux calibrations), σ_r , uncertainties due to the extinction correction, σ_e . The final uncertainty for each line was determined from

$$\sigma = \sqrt{\sigma_c^2 + \sigma_r^2 + \sigma_e^2}$$

These uncertainties were measured for each line ratio at each spectrum in all the positions for each galaxy. With these values a total uncertainty for each line and each slit position can be determined. They are given in Table 2.

3. Diffuse Ionized Gas

As mentioned above, we are interested in the study of the spectral characteristics of the DIG. They will be used to understand the ionization source of this gas and the nature of the H II regions.

The best parameter to discriminate between ionized gas inside and outside the H II regions is the density. Unfortunately, density is one of the most difficult parameters to determine from long-slit spectroscopy data. The main problem is that in the low-density regime the differences in the $[\text{S II}]\lambda 6717/[\text{S II}]\lambda 6731$ ratio, which is the most common line ratio used in the density determination, between H II regions, with typical densities of 100 cm^{-3} , and the DIG, with values of 10 cm^{-3} , are about 0.1 (see Figure 5.3 in Osterbrock 1989). Such a difference is normally smaller than the uncertainties in the ratios themselves. In spiral galaxies this can be overcome by studying the gas above the disc (e.g. Otte & Dettmar 1999) or in the inter-arm region (Benvenuti et al. 1976), with neither of them clearly defined for irregular galaxies. Therefore, other parameters have to be used in the study of the DIG. In this sense the emission measure (EM), related to surface brightness in $\text{H}\alpha$ and the electronic temperature (Greenawalt et al. 1998), is a good choice. In the Milky Way there is a correlation between low EM and low density (R. Reynolds 2004, private communication). Therefore, the EM can be used to discriminate between DIG and H II regions when the density cannot be determined. The main problem is the lack of a unique value for the EM of the DIG in spiral galaxies. It varies from 80 pc cm^{-6} in the arms of spiral galaxies (Hoopes & Walterbos 2003) to 2 pc cm^{-6} in the Milky Way (Reynolds 1989). Instead of choosing a value in this range, we decided to use another approach. The cumulative distribution function of the surface brightness in $\text{H}\alpha$ [hereafter $\text{SB}(\text{H}\alpha)$] is a smoothly increasing function with a change in the slope when H II regions begin to dominate the light. This break point in $\text{SB}(\text{H}\alpha)$ can be considered as the limiting value between DIG and H II regions. This procedure has already been used for some galaxies (IC 10, Hidalgo-Gómez 2005; NGC 6822, Hidalgo-Gómez & Peimbert 2007; Gr 8 and ESO 245-G05, Hidalgo-Gómez 2006). Figure 1 shows the cumulative function of $\text{SB}(\text{H}\alpha)$ obtained from the 1D spectra, and corrected for Galactic extinction following Schlegel et al. (1998). The break point is

located at 5×10^{-18} ergs s⁻¹ cm⁻² arcsec⁻², which corresponds to a flux of 5.45×10^{-17} ergs s⁻¹ cm⁻². This value is very similar to the ones found in GR 8 and ESO 245-G05 (Hidalgo-Gómez 2006). In their study of the H II regions in DDO 53, Strobel et al. (1990) set the boundaries of their regions at a flux of 5×10^{-17} ergs s⁻¹ cm⁻², which is very similar to the value found here. Another break point can be detected at 3.2×10^{-21} ergs s⁻¹ cm⁻², arcsec⁻² which might be an indication of noise level. There are only five data points with SB(H α) lower than this limit, and they are not going to be considered in this investigation.

Using this SB(H α) from the 1D spectra, we can divide the data points into 58 DIG and 13 H II locations. Another 10 spectra have no emission in any line. In addition to the 1D spectra, we can sum up all the rows with SB(H α) lower (higher) than 5×10^{-18} ergs s⁻¹ cm⁻² arcsec⁻² in order to create the so-called “integrated spectra” for the DIG (H II regions). A total of 26 integrated spectra were created: 9 H II regions and 17 DIG locations.

The main caveat is that the cumulative function is a statistical approach, and therefore, the distinction between H II regions and DIG might be fuzzy, especially at low surface brightness or when the spatial averages of the 1D spectra are large, as in NGC 6822, where the 1D spectra covered 50 pixels (see Hidalgo-Gómez & Peimbert 2007 for details). In order to test the goodness of this approach, we can study the relation between SB(H α) and the line ratios, particularly the [O III]/H β and [S II]/H α ratios. This is shown in Figure 2. As expected, there is a trend toward low [S II]/H α and high [O III]/H β as SB(H α) gets larger, with regression coefficients of -0.45 and -0.3 , respectively. The transition between H II and DIG locations is very smooth in the log [O III] versus SB(H α) plot, although the dispersion is large. There are DIG locations with high excitation (> 2) and H II regions with low excitation (< 1). Two of the latter are located at the border of the H II regions, and therefore, they might share the characteristics of both locations, while another two are small H II regions of only 1D spectra. Finally, the DIG with the highest excitation corresponds to slit f, where no H II regions were detected. The transition in Figure 2b is also smooth, with a very steep correlation for the DIG locations. In any case, these figures indicate that the distinction made in this investigation is reasonable.

3.1. Line Ratios along the Slits

Once the distinction between the H II regions and the DIG locations is clear, the next step is to study some of the characteristics, such as the excitation, the distribution of SB(H α), and the ratios [N II]/H α and [S II]/H α throughout the galaxy. This can be performed using the set of 1D spectra previously defined. Each of the 1D spectra covers 90 pc, and therefore, the variations between them for the H II and DIG locations can be studied in detail.

Figure 3 shows the variations of SB(H α) along the slit, from north (at the top, slit a) to south (slit h) and from west (to the left) to east. All the slit positions have the same SB limits in order to see their differences throughout the galaxy. Those places with SB(H α) higher than 5×10^{-18}

ergs s⁻¹ cm⁻² arcsec⁻² (H II regions) are contained between dot-dashed lines. The most extended H II regions are located at slits b, c and d, with sizes of 315, 360, and 315 pc, respectively. As we move towards the south the H II regions get smaller and the DIG is more extended. In fact, in one slit position (f) there are no H II regions. When compared with an H α image (e.g. Figs. 2a and 2b in Strobel et al. 1990), the similarities are clear. The largest H II regions are located in the north of the galaxy, while towards the south, only small clumps of high intensity are found with a lot of ionized gas among them. The regions in this investigation can be identified as regions No 9 (slit a), No 10 at slit b, No 13 at slits c and d, No 5 and 11 (e), No 8 and 16 (g) and No 17 at slit h in Strobel et al. (1990). It has to be kept in mind that the slit positions are not next to each other, with spatial gaps between the slits. Moreover, the slits were offset towards the west when moving from north to south following the orientation of the galaxy. It is interesting to note that there are no abrupt changes in SB(H α) from the H II regions towards the DIG, as in NGC 6822 (see Fig. 3 in Hidalgo-Gómez & Peimbert 2007).

The [O III]/H β ratio along the slits is shown in Figure 4. The orientation and the meaning of the lines are the same as in Figure 3. Along with the H II regions, the values from the integrated spectra are shown as dotted lines. No uncertainties are shown for the sake of clarity. Also, the limits in all the slit positions are the same in order to see any differences among them. The largest value of the excitation of 3.38 ± 0.01 is at slit h, corresponding to region No 17, while slits b, c and d show [O III]/H β between 2.5 and 3. They coincide with the largest and brightest H II regions of the galaxy. The largest value of the excitation is normally coincident with the largest SB except for slit e, where the maximum excitation is at the border of one of the H II regions. Moreover, the excitation inside the H II regions of slit e is very low (≤ 1 in both cases) and very similar to the values outside them. On the contrary, the excitation is very high (≥ 1) for most of the DIG locations of slit f. Both slit g and h are normal, with the highest excitation inside the H II regions and a low value of the excitation outside them, in general. Concerning the DIG, it is well known that the [O III]/H β ratio is lower than 1 in the DIG of spiral galaxies (Rand 1998). This is not the situation here, since most of the values of this ratio are larger than 1 at the DIG. In fact, three of the 1D spectra of slit f, where no proper H II regions are, have [O III]/H β larger than 2. Such large values of this ratio for DIG locations have been measured in other dwarf irregular galaxies, such as IC 10 (Hidalgo-Gómez 2005), NGC 6822 (Hidalgo-Gómez & Peimbert 2007), and ESO 245-G05 (Hidalgo-Gómez 2006). Another interesting fact to note is that only for slits b, c, g, and h is this ratio larger inside the H II regions than in the DIG locations, as expected. For the rest of the slits (a, d, and e), the value of the ratio in the DIG is smaller than or of the same order as inside the H II regions. For all of them, the [O III]/H β ratio from the 1D spectra agrees with the values from the integrated spectra when the uncertainties are considered.

Figure 5 shows the [S II]/H α ratio along the slit positions. The orientation and the meaning of the lines are the same as in Figure 3, and the values are between 0 and 0.5 for all slit positions. Again, the average values are shown as dotted lines, when determined. In previous studies an important difference in this ratio between the DIG and the H II locations has been detected for

both spiral (NGC 55; Otte & Dettmar 1999) and irregular galaxies (NGC 6822; Hidalgo-Gómez & Peimbert 2007). It is very interesting to note that, in general, there is no such difference here, either in the integrated spectra or in the 1D ones, with similar values of the $[\text{S II}]/\text{H}\alpha$ ratio in the DIG and inside the H II regions (e.g. slits a, c and d). For those slit positions where the differences are larger, they are not as large as in other irregular galaxies, such as NGC 6822 (Hidalgo-Gómez & Peimbert 2007). In fact, a very large value of this ratio is detected inside the H II region gh2 for both the 1D spectra and the integrated ones, which is quite unexpected. Moreover, sulfur lines were not detected at any locations along slit b but, due to the larger S/N, a value is obtained from the average spectrum. On the contrary, $[\text{S II}]/\text{H}\alpha$ is measurable in two of the 1D spectra of slit h, but no value could be obtained for the average spectrum because the number of 1D spectra where this line is not detected was larger than the number of locations where it is detected. In this case, the noise from the non detections is larger than the signal.

The $[\text{S II}]/\text{H}\alpha$ ratio is important because it might be a shock indicator (Dopita 1993). For low metallicities, intensities larger than 0.3 indicate the existence of shocks (Stasińska 1990) when the excitation is low. Such large values are not observed except for a total of four 1D spectra in slits e, f and g, and none of them has a high excitation as well. Three of them are located in the eastern part of the galaxy. Begum et al. (2006), in their study of the interstellar medium of this galaxy, obtained velocity maps. They found out that the velocity gradient towards the south eastern part of the galaxy, which is receding from us, is larger than that in the northern approaching half of the galaxy. Apart from this, there is nothing else peculiar in the H I and velocity maps. An increment in the $[\text{S II}]/\text{H}\alpha$ ratio towards the south is clearly seen in Figure 5, which might resemble the increase in the velocity gradient. In this sense, the lack of this ratio in the southernmost slit position, h, is even more intriguing. From this information it can be advanced that shock might not be important as an ionization source, as we discuss in section 4, in spite of the disturbed kinematics of the galaxy (Begum et al. 2006).

The $[\text{N II}]/\text{H}\alpha$ ratio is not shown here due to the small number of 1D spectra where nitrogen was detected. Therefore, few conclusions could be obtained from this distribution. The few points detected in the northern slits have very low values of this ratio, while they increase when moving towards the south, with ratios of 0.3 at slit e.

Finally, Figure 6 shows the extinction along the slits. It is parametrized with the extinction coefficient defined as in Section 2. The values are corrected for Galactic extinction following Schlegel et al. (1998). DDO 53 shows an irregular extinction distribution, not only along the slits but also between them. There are slits where the extinction seems to be very homogeneous (e.g. a-d), while slits e-h show (extended) clumps of it, as can be seen in the $\text{H}\alpha$ image from Strobel et al. (1990). This might resemble the fact that at this part of the galaxy the H II regions also have small sizes, while at the northern part the H II regions have larger sizes. This behaviour is very similar to that of other galaxies, such as GR 8 (Hidalgo-Gómez 2006). As in IC 10 (Hidalgo-Gómez 2005) and GR 8 (Hidalgo-Gómez 2006), the larger extinction is not associated with the H II regions and vice versa. The maxima are located at e6 and f6 with values of 6 ± 1 and 5 ± 1 , respectively. They

are not associated with the two clumps observed in H I (Begum et al. 2006), and they are mainly coincident with the northern regions, No 9 and No 10, and the south eastern ones No 17 and 18. In any case, it is interesting to note that most of the values of C_β are larger than 1. This is contrary to the idea that dwarf galaxies are almost dust-free (Lee et al. 2003) and in agreement with the conclusions from high spatial resolution investigations carried out in the Small Magellanic Cloud by Caplan et al. (1996).

3.2. The Integrated Spectra

As previously said, in addition to the 1D spectra, average spectra were obtained for each slit position. For them, the lines [O III] λ 5007 and [S II] λ 6717, as well as H β and H α , were measured. In Table 3, along with the line ratios [O III]/H β and [S II]/H α , the extinction coefficient C_β and the S/N in H α for the integrated spectra are shown. Also, in order to make a quick comparison with models, the [O III]/H α ratio is presented. [N II] λ 6583 was detected in only bh1, while He I λ 6678 was detected in bh1 and ch1, but the values are not presented in the table.

The DIG results obtained from the integrated spectra are very similar to those from the 1D spectra: large values of the [O III]/H β ratio, low values of [S II]/H α , and large extinction. Concerning the [O III]/H β ratio, half of the DIG locations have values lower than 1, but none of them have values lower than 0.5, which is the highest value measured at the DIG in spiral galaxies (Rand 1998). The differences in the [O III]/H β ratio between irregular galaxies and the extraplanar DIG in spiral galaxies indicate higher oxygen abundances in irregular galaxies or harder spectra. Most of the low excitation values in DDO 53 correspond to the southern slits (e-g). On the contrary, for the northern slits half of the DIG locations have values of [O III]/H β larger than 1.5. We have to keep in mind that these slits pass through the most luminous H II regions of the galaxy, regions No 10 and 13 (Strobel et al. 1990). Such large values of the [O III]/H β ratio are also measured for the DIG of other irregular galaxies, such as IC 10 (Hidalgo-Gómez 2005). If the absorption-corrected ratios are considered, the [O III]/H β ratio is lower: in general, 50% lower than the values presented in Table 3.

We also present the [O III]/H α ratio. As previously said, this ratio is given because it is widely used in modelling, despite its strong dependence on extinction. Therefore, the values presented here should be taken with care. It has been observed that this ratio gets larger with the distance from the galactic plane (Otte et al. 2002), with values larger than 0.3 outside the H II regions. Values larger than these are observed here for almost all DIG locations and H II regions. If no extinction correction is made, the values are even larger. Also, there are no significant changes ([O III]/H α lower than 0.3) if any of the absorption corrections discussed in Section 2 are performed.

There are a few things to be noted in relation to the [S II]/H α ratio from Table 3. First, the values inside and outside the H II regions are very similar, as noted for the 1D spectra, and to the contrary of what was found for other galaxies (e.g. NGC 6822; Hidalgo-Gómez & Peimbert 2007).

Second, the values increase towards the south (the receding, disturbed part of the galaxy), with a maximum at gh2, which is an H II region. Eight out of nine integrated spectra where sulfur is detected in the southern region have $[\text{S II}]/\text{H}\alpha$ larger than 0.1, as compared to only 3 out of 10 in the northern region of DDO 53. The larger gradient of the velocity towards the south of the galaxy (Begum et al. 2006) might be an indication of a disturbance, which might create a shock wave. As for higher velocities of the gas the shocks are more important, and this ratio will be larger. These results confirm the trend observed in the 1D spectra. An average value of 0.147 could be obtained for the $[\text{S II}]/\text{H}\alpha$ ratio considering all the DIG integrated values. This is the second lowest value of this ratio for the sample of galaxies already studied, slightly lower than for ESO 245-G05 and GR 8 (0.165) and much lower than for IC 10 (0.31). The low value of the $[\text{S II}]/\text{H}\alpha$ ratio might indicate that although the interstellar medium is disturbed, there is no evidence for shocks (see Section 4.1). Again, when the absorption-corrected ratios are used instead, the $[\text{S II}]/\text{H}\alpha$ ratio is, on average, 40% lower than those discussed here, but the general trend remains.

Finally, the extinction also follows the same trend that was observed in the 1D spectra. DDO 53 has a significant amount of dust. There are locations with C_β larger than 2, and there is no systematic trend of the H II regions being dustier than the DIG or vice versa. It is important to note that the southern regions seem to be dustier than the northern ones.

4. The ionization source

In order to determine the ionization source of the DIG, a comparison can be made between the line ratios measured in this galaxy and the values predicted by different models. Considering radiation-bounded H II regions, Mathis (1986) and Domgörgen & Mathis (1994) obtained that the value of both $[\text{S II}]/\text{H}\alpha$ and $[\text{N II}]/\text{H}\alpha$ for the DIG are very large, larger than 0.3, while $[\text{O III}]/\text{H}\alpha$ is lower than 0.1. The main caveat is that these results are optimized for Milky Way metallicities. As discussed in the next section, the metallicity of DDO 53 is much lower than the Milky Way's. Castellanos et al. (2004) tried to reproduce the line ratios of the DIG for low-metallicity galaxies using the photoionization code CLOUDY. They successfully reproduced the increase of both $[\text{N II}]/\text{H}\alpha$ and $[\text{S II}]/\text{H}\alpha$, but they did not fit the excitation, $[\text{O III}]/\text{H}\beta$. Wood & Mathis (2004) performed Monte Carlo simulations of a multicomponent interstellar medium with different ionizing spectra and metallicities in order to explain the increase of the $[\text{N II}]/[\text{S II}]$ ratio with the distance from the plane. They fit this ratio but not others, such as $[\text{O III}]/\text{H}\alpha$. Comparing the value listed in Table 3 with the results from Mathis (1986) and Domgörgen & Mathis (1994), it can be concluded that the H II regions in DDO 53 are not radiation-bounded because $[\text{O III}]/\text{H}\alpha$ is never as low as 0.1, and $[\text{S II}]/\text{H}\alpha$ never as high as 0.3 except in gh2. Actually, the lowest $[\text{O III}]/\text{H}\alpha$ value is 0.20 (ed2 and ed3).

In recent years density-bounded H II regions have been modelled (Wood & Mathis 2004; Hoopes & Walterbos 2003), but again for high-metallicity regions. Therefore, some corrections have to be made. The real corrections cannot be done, but one knows that lower metallicities imply a high

ionization parameter, which implies higher $[\text{O III}]/\text{H}\beta$ ratios. Therefore, the lower the metallicity, the higher the $[\text{O III}]/\text{H}\beta$ ratio for similar T_{ion} . As a consequence, the photon leakage obtained from the models might be larger than the real leakage, or T_{ion} lower than the real value.

We compare the values listed in Table 3 with those from the Hoopes & Walterbos (2003) model. This model is preferred because Wood & Mathis (2004) focus on explaining the rising relation between $\log [\text{N II}]/\text{H}\alpha$ and $\log [\text{S II}]/\text{H}\alpha$ for the DIG. $[\text{N II}]$ is not detected except in a few regions of the DIG in DDO 53, and such a relationship cannot be studied.

Table 4 shows the leakage of photons from the H II regions needed for each of the line ratios measured for the integrated DIG spectra from the Hoopes & Walterbos models. The corresponding ionization temperatures are also listed. First, we can study the results from the $[\text{S II}]/\text{H}\alpha$ ratio. Ionization temperatures lower than 40,000 K and photon leakages lower than 40% are obtained from them in all the locations where it was detected but two (gd3 and fd1). On the contrary, the T_{ion} values which fit the $[\text{O III}]/\text{H}\beta$ ratios are always higher than 38,000 K. Photon leakages larger than 40% are the most common value. Considering that the metallicity of DDO 53 is lower than the metallicity of Orion, for which the model is calculated (see section 5.1), the values for the $[\text{O III}]/\text{H}\beta$ ratio might be upper limits. Therefore, considering the uncertainties of the ratios and the difference in metallicity, a T_{ion} between 38,000 and 41,000 K fits very well both ratios for all slit positions. Also, values of photon leakages between 35% and 50% can account for both ratios in all slits but gd2, where larger leakage is needed. Moreover, all slits but a and b show a good agreement in T_{ion} between all the DIG locations inside the slit. The photon leakage range is broader, and therefore more difficult to be fitted by a single value.

These ionization temperatures seem quite realistic, as can be seen from Figure 7, where the $\log [\text{S II}]/\text{H}\alpha$ versus $\log [\text{O III}]/\text{H}\beta$ diagram is shown. Superimposed on the data points (both H II regions and DIG locations) are tracks of ionization temperature from Figure 3 in Martin (1997). The tracks indicate the temperatures needed to ionize the medium only by photoionization for a metallicity of $0.20 (O/H)_{\odot}$. These are 50,000 K (*solidline*) and 35,000 K (*dashedline*). Most of the DIG data points have T_{ion} between 35,000 and 42,000 K while one DIG locations have T_{ion} higher than 42,000 K (fd1) and three of them have ionization temperatures lower than 35,000 K (bd2, gd1, and ed2). Location fd1 has a very large excitation, and therefore, it is located in that position in the diagram. Moreover, two H II regions (gh2 and eh1) have extreme ionization temperatures, larger than 50,000 K and lower than 35,000 K, respectively. Such values are very unlikely for normal H II regions. Their excitations are normal as compared to the values of the other H II regions, but they have the highest and the lowest $[\text{S II}]/\text{H}\alpha$ ratios (see Table 3), and therefore, they occupy these positions in the $\log [\text{S II}]/\text{H}\alpha$ versus $\log [\text{O III}]/\text{H}\beta$ diagram. From Figure 7 it is also interesting to note that there is no real difference in the ionization temperatures between H II regions and DIG locations.

It can be concluded that most of the locations agree with T_{ion} values between 35,000 and 41,000 K and photon leakages between 35% and 50%. The uniformity of these values is very

interesting, indicating similar conditions throughout the galaxy. There cannot be a single value for the whole galaxy, as physical conditions vary throughout it. Moreover, they are independent of absorption correction, in the sense that the same values are obtained for the T_{ion} and leakage percentages when the absorption-corrected ratios are considered. With these values, and following Vacca et al. (1996), the stars responsible for the ionization are of types O7-O9, with masses between 20 and 30 M_{\odot} .

4.1. Other Sources of Ionization?

As we said before, photon leakages from H II regions seem to be the main ionization source of the DIG in DDO 53. In any case, it might be interesting to look for other ionization sources.

Turbulent mixing layers (TMLs) are good candidates in the sense that the low-ionization lines, such as [S II] $\lambda 6717$, are the most affected by such mechanisms. Shear flows at the boundaries of hot and cold gas produce intermediate-temperature gas ($T \approx 10^5$) that radiates strongly in the optical, ultraviolet, and extreme-ultraviolet. By including the effects of non-equilibrium ionization and self-photoionization of the gas as it cools after mixing, the intensity of some lines in the optical, infrared, and ultraviolet can be predicted. In Figure 8 we have plotted the data points for DDO 53 along with the TML model by Slavin et al. (1993) as a dashed line, the radiation-bounded model (*dottedline*), and the density-bounded model (*solidline*) from Rand (1998). The dispersion is large, especially when H II regions are considered, but it can be concluded that TML is not playing a part in DDO 53, as expected. It is interesting to see that all the data points are between the density-bounded and the radiation-bounded lines, as expected. The slope of the DIG data points (-0.395) is closer to the slope of the density-bounded model (-0.439). On the contrary, the slope of the H II regions is very different (0.257). In addition, it can be seen that most of the data points agree with an ionization factor of $q \leq -3.5$, in agreement with the value we used in the Hoopes & Walterbos model of -3 [q is related to the ionization parameter as $U = 0.0013(T/10^4)^{-0.55}q^{1/3}$ according to Hoopes & Walterbos (2003)].

Finally, it might be interesting to explore the existence of shock waves, which might have some influence on the ionization. As previously said, the interstellar medium of this galaxy seems to be quite disturbed, with a gradient in the velocity increasing towards the south. Such disturbances might create shock waves which can be amplified along the galaxy. As we previously discussed, there is only one location where the [S II]/ $H\alpha$ ratio is larger than 0.3 (7h1). In any case, the best way to check the existence of shocks is the diagnostic diagram $\log[S II]/H\alpha$ versus $\log[O III]/H\beta$ (Veilleux & Osterbrock 1987). Figure 9 shows both the DIG and H II region data points. To the left of the solid line there is the photoionized region, and to the right the shocked region. Only one H II region (gh2) is in this latter part of the diagram. The rest of the locations are in the photoionization region. Therefore, it can be concluded that shocks are not important in this galaxy despite the disturbances of the interstellar medium.

5. Discussion

From the discussion in the previous section it is obvious that leakage photons from the H II regions are the main cause of the ionization of the DIG in DDO 53. The values of the leakage are between 35% and 50%, which are similar to those in other dwarf irregular galaxies. No other ionization sources (shock waves, mixing layers, etc) seem to be at work in this galaxy.

We can compare the line ratios obtained in DDO 53 with those from other galaxies studied so far. The DIG [S II]/H α ratio is very similar in all the galaxies, with values of 0.12-0.16 except IC 10 (0.31; Hidalgo-Gómez 2005). On the contrary, the DIG excitation changes a lot from galaxy to galaxy. The larger value corresponds to IC 10 (1.66), but both NGC 6822 and DDO 53 have values very similar to this one. The lowest excitation corresponds to ESO 245-G05 (0.81; Hidalgo-Gómez 2006). These high values of the excitation can be due to differences in the oxygen content or in the ionizing spectra. DDO 53 has a very similar oxygen content to ESO 245-G05 of $12+\log(\text{O}/\text{H}) = 7.8$, but their [O III]/H β ratios are very different. As we said, the value in DDO 53 is similar to those in NGC 6822 and IC 10, which are much more metallic. Therefore, differences in the metallicity cannot account for the differences in excitation. A harder spectrum might indicate more massive, hotter stars. As a consequence, the H II regions might be larger and more luminous. Strobel et al. (1990) concluded that the value of the slope of the luminosity function in H α is similar to those found in other irregular galaxies, such as NGC 6822, IC 10, and GR 8. They reached a similar conclusion on the sizes of the H II regions. These four galaxies have very similar values of the DIG [O III]/H β ratio, indicating that their ionizing spectra are very similar. Therefore, it can be concluded that the excitation values at the DIG are more closely related to the ionizing spectra than to the oxygen content.

5.1. The Metallicity of DDO 53

In addition to the study of the DIG we can determine the chemical abundances in DDO 53 from the intensities of the integrated H II spectra. The main caveat is the low efficiency of the Boller&Chives spectrograph below 4000 Å. As mentioned previously, it is less than 10%. Therefore, although the intensities of the lines below 4000 Å could be detected, the values might not be very realistic. For example, the corrected intensity of the [O II]/H β ratio of region ch1 is 0.20, which is very low when compared with the values in other H II regions in dwarf irregular galaxies (see Hidalgo-Gómez & Olofsson 2002). Therefore, in order to obtain more reliable intensities of the [O II] lines, equation (1) in Hidalgo-Gómez & Ramirez-Fuentes (2007) is used. This equation relates the intensities of [O II] λ 3727 and [O III] λ 5007. The reliability and uncertainties of this equation are discussed in Hidalgo-Gómez & Ramirez-Fuentes (2007). In this case, we feel that the values obtained from this equation are more trustworthy than those measured in the spectra, and these will be the values used in the determination of the chemical abundances presented here.

In two of these H II integrated spectra, the forbidden oxygen line [O III] λ 4363 is present, so

we can obtain a reliable determination of the electron temperature and the chemical abundances following the so-called standard method (Osterbrock 1989). These two spectra are regions *2h1* and *3h1* in Table 2, which correspond to regions No 10 and No 13 in Strobel et al. (1990). The intensities of all the lines measured, extinction- and absorption-corrected, are given in Table 5, along with their uncertainties.

The determined oxygen and nitrogen abundances for regions No 10 and No 13 are presented in Table 6, along with the electronic temperature of the O^{++} (inner) and the N^+ (outer) zones. The oxygen abundances obtained here of 7.80 ± 0.1 and 7.91 ± 0.3 agree with the values of ≈ 7.8 obtained with semiempirical methods (I. Saviane 2004, private communication), but they are slightly higher than the previous values obtained for this galaxy of 7.62 (Skillman et al. 1989). In any case, DDO 53 is a low-metallicity galaxy. It is confirmed by the low nitrogen abundance of $12 + \log(N/H) = 5.7$. Moreover, nitrogen is not detected in region No 13. None of the previous determinations of the abundances of DDO 53 measured nitrogen; therefore, a comparison cannot be made. This value is even lower than for DDO 190 [$12 + \log(N/H) = 5.97$; Hidalgo-Gómez & Olofsson 2002] which is the galaxy with the lowest nitrogen abundance in a sample of dwarf irregular galaxies. Moreover, the $\log(N/O)$ ratio is also very low, only -2.12 , which is very much lower than the canonical -1.5 obtained for a sample of blue compact and irregular galaxies (Izotov & Thuan 1999). These low nitrogen abundances might explain the lack of this line in the majority of the H II regions and DIG locations. Such low values of nitrogen have been observed in other dwarf irregular galaxies, such as GR 8 [$\log(N/O) = -1.77$; Moles et al. 1990].

Finally, we can also determine the helium abundance. Only one line is used (He I at 6678 Å), because the intensities of other lines can be polluted by sky lines (He I at 5578 Å) or by processes other than pure recombination (He I at 4471 Å; Izotov & Thuan 2004). Moreover, as the most reliable ionization correction factor is based on the intensity of [S III] lines, which are not present in our spectra, the He^+/H^+ ratio is given. The values of both regions No 10 and No 13 are equal to 0.11, very similar to that of other galaxies of the same type (Hidalgo-Gómez 1999).

The abundances of these three elements follow a similar pattern to those of DDO 190, with very low nitrogen and low oxygen but normal helium values (see Table 3 in Hidalgo-Gómez & Olofsson 2002).

Another interesting problem is the (in)homogeneity of the chemical abundances in dwarf irregular galaxies. Only in three galaxies have enhancements of oxygen (IC 4662 and ESO 245-G05; Hidalgo-Gómez et al. 2001) or nitrogen (NGC 5253; Kobulnicky et al. 1997) been reported. We might use the values presented here to study the oxygen distribution along DDO 53. Regions No 10 and No 13 are quite close to each other, and their oxygen and helium abundances are similar considering the uncertainties. In order to enlarge the number of oxygen determinations we can use the other seven H II regions defined in Section 3.1. Again, the [O II] $\lambda 3727$ intensity can be obtained from equation (1) in Hidalgo-Gómez & Ramírez-Fuentes (2007). With the intensities, reddening-corrected and normalized to $H\beta$, of [O II] $\lambda 3727$, [O III] $\lambda 4959$, and [O III] $\lambda 5007$, any of the

semiempirical methods, the R_{23} (Pagel et al. 1979) or the P method (Pilyugin 2000, 2001), can be used to determine the oxygen abundance. The values are shown in Table 7 along with the uncertainties. These uncertainties take into account the intrinsic uncertainties of the methods themselves due to their statistical nature. Such uncertainties might be 0.2 dex according to Hidalgo-Gómez & Ramírez-Fuentes (2007). Considering all the uncertainties, the oxygen abundances reported in Table 7 should be considered as a first approximation only. In consequence, few conclusions can be obtained. First, DDO 53 seems to be a low metallicity galaxy. But at the center of the galaxy, the metallicity seems to be even lower (regions No 5, No 6, and No 11) than in the rest of the H II regions, the difference being 0.6 dex, much larger than the uncertainties. In order to clarify this point, new measurements with good resolution and high S/N ranging from [O II] $\lambda 3727$ to [S II] $\lambda\lambda 6717, 6731$ are needed in order to get a better determination of the abundances throughout the galaxy. Such observations would throw light on this situation.

6. Conclusions

We studied the line ratios of the DIG in the dwarf irregular galaxy DDO 53 using long-slit spectroscopy. The DIG values were compared with those of the H II regions. In order to do this comparison, definitions of H II regions and the DIG were made based on the flux of the H α line. With this definition we divided the data into 9 H II regions and 17 DIG locations. The differences in the line ratios among them are less extreme than for other dwarf irregular galaxies studied before, such as NGC 6822 (Hidalgo-Gómez & Peimbert 2007) and IC 10 (Hidalgo-Gómez 2005). The excitation is as large in this galaxy, especially at the DIG location, as in other galaxies, indicating similar ionizing spectra. On the contrary, the [S II]/H α ratio is lower than in the previously studied galaxies. [N II] $\lambda 6583$ is detected in very few locations along the slits and is not studied here. In addition to the line ratios, the extinction is studied along the slit positions, indicating that the dust inside the northern part of the galaxy is more homogeneously distributed than in the southern part, where large clumps of dust are clearly detected.

The line ratios obtained are consistent with density-bounded H II regions with a photon leakage of 35% -50% and ionization temperatures between 35,000 and 42,000 K for most of the locations. No other sources of ionization (shocks, turbulence, etc.) are needed in order to explain the line ratios observed in spite of the disturbed kinematics of the galaxy in H I (Begum et al. 2006).

Finally, we determined the abundances for two H II regions using the electron temperature method. The values are very similar and indicate that this is a low-metallicity galaxy. When semiempirical methods are used to determine the oxygen abundances for a large number of H II regions, a difference towards the center of the galaxy is obtained, indicating possible inhomogeneities in the oxygen content. In any case, new spectra are needed in order to confirm this trend.

The author is indebted to Nahiley Flores-Fajardo for preparing Figure 8. She thanks G. García-Segura for interesting discussions. The anonymous referee is thanked for interesting comments and

discussion which have improved this manuscript. She also thanks J. Brennan for a careful reading of the manuscript. This investigation is supported by DGAPA project IN114107.

REFERENCES

- Begum, A., Chengalur, J.N., Karachentsev, I.D., Kaisin, S.S., & Sharina, M.E. 2006, MNRAS, 365, 1220
- Benvenuti, P., D’Odorico, S., & Peimbert, M. 1976, RevMexA&A, 2, 3
- Brocklehurst, M. 1971, MNRAS, 153, 471
- Caplan, J., Ye, T., Deharveng, L., Turtle, A.J., & Kennicutt, R.C. 1996, A&A, 307, 403
- Castellanos, M., Valls-Gabaud, D., Díaz, A. & Tenorio-Tagle, G. 2004, ”How does the Galaxy work ? “ eds: E.J. Alfaro, E. Pérez & J. Franco, Kluwer Academic Publishers, p. 101
- Dömgonge, H. & Mathis. J.S. 1994, ApJ, 428, 647
- Dopita, M. A. 1993, PASAu, 10, 359
- Greenawalt, B., Walterbos, R.A.M., Thilker, D. & Hoopes, C.G. 1998, ApJ 506, 135
- Hidalgo-Gómez, A.M. 1999, Ph.D. Thesis, Uppsala University
- Hidalgo-Gómez, A.M., 2005, A&A 442, 443
- Hidalgo-Gómez, A.M. 2006, AJ, 131, 2078
- Hidalgo-Gómez, A.M., & Olofsson, K. 1998, A&A, 334, 45
- Hidalgo-Gómez, A.M., Masegosa, J., & Olofsson, K. 2001, A&A, 369, 797
- Hidalgo-Gómez, A.M., & Olofsson, K. 2002, A&A, 389, 836
- Hidalgo-Gómez, A.M. & Peimbert, A. 2007, AJ, 133, 1874
- Hoppes, C. G. & Walterbos, R.A.M. 2003, ApJ, 586, 902
- Hunter, D.A. & Gallagher, J.S. III 1992, ApJ, 391, 9
- Hunter, D.A. & Elemegreen, B.G. 2004, AJ, 128, 2170
- Izotov, Y.I. & Thuan, T.X. 1999, ApJ, 511, 639
- Kobulnicky, H.A., Skillman, E.D., Roy, J-R., Walsh, J.R., & Rosa, M.R. 1997, ApJ, 477, 679
- Lee, H., McCall. M.L. & Richer, M.G. 2003, AJ, 125, 2975

- Martin, C.L. 1997, *ApJ*, 491, 561
- Mathis, J.S. 1986, *ApJ*, 301, 423
- McCall, M.L., Rybski, P.M., & Shields, G.A. 1985, *ApJS*, 57, 1
- Moles, M., Aparicio, A., & Masegosa, J. 1990, *A&A*, 228, 310
- Olofsson, K. 1995, *A&AS*, 111, 57
- Osterbrock, D.E. 1989, *Astrophysics of Gaseous Nebulae and Active Galactic Nuclei*, (University Science Books, Mill Valley, CA)
- Otte, B. & Dettmar, R.-J. 1999, *A&A*, 343, 705
- Otte, B., Gallagher, J.S.III, & Reynolds, R.J. 2002, *ApJ*, 572, 823
- Pagel, B.E.J., Edmunds, M.G., Blackwell, D.E., Chun, M.S., Smith, G. 1979, *MNRAS*, 189, 95
- Pilyugin, L.S. 2000, *A&A*, 362, 325
- Pilyugin, L.S. 2001, *A&A*, 369, 594
- Rand, R.J. 1998, *ApJ*, 501, 137
- Rand, R.J., Kulkarni, S.R. & Hester, J.J. 1990, *ApJ*, 352, 1
- Reynolds, R.J. 1983, *ApJ*, 268, 698
- Reynolds, R.J. 1989, *ApJ*, 345, 811
- Savage, B.D. & Mathis, J.S. 1979, *ARA&A*, 17, 73
- Schlegel, D.J., Finkbainer, D.P., & Davis, M. 1998, *ApJ*, 500, 525
- Schuster, W.J., & Parrao, L. 2001, *RevMexA&A*, 37, 187
- Slavin, J.D, Shull, J.M. & Begelman, M.C. 1993, *ApJ*, 407, 83
- Stasinska, G. 1990, *A&A*, 83, 501
- Strobel, N.V., Hodge, P., & Kennicutt, R.C. 1990, *PASP*, 102, 1241
- Vacca, W.D., Garmany, C.D., & Shull, J.M., 1996, *ApJ*, 460, 914
- Veilleux, S. & Osterbrock, D.E. 1987, *ApJS*, 63, 295
- Wood, K., & Mathis, J.S. 2004, *MNRAS*, 353, 1126

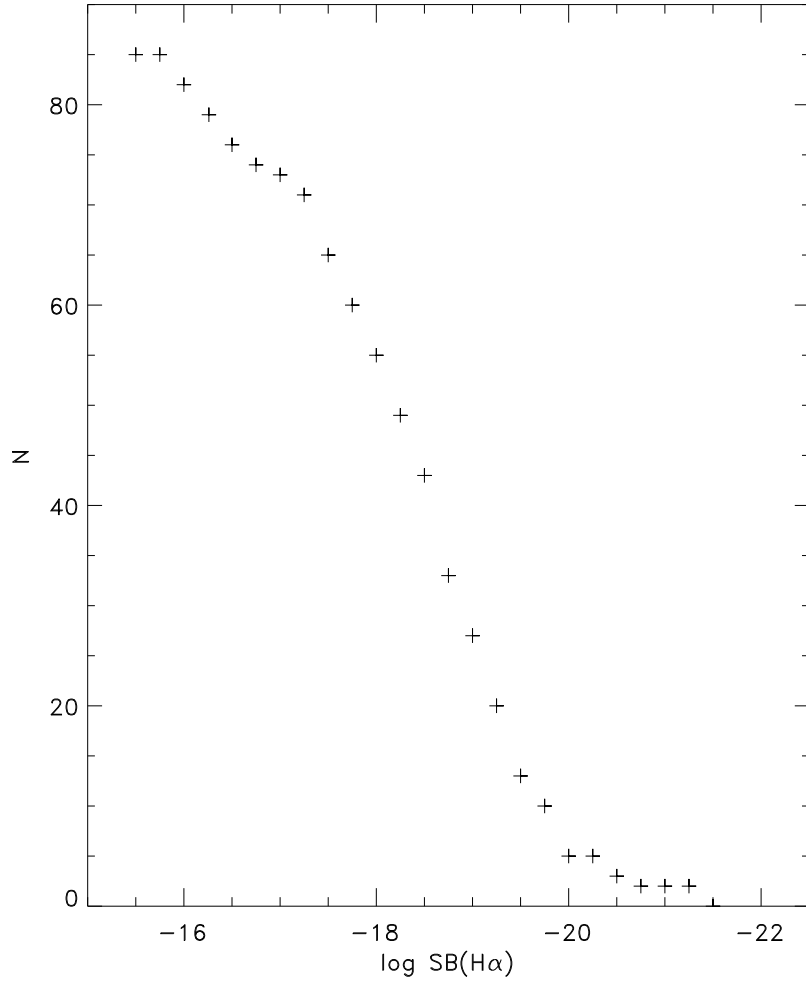


Fig. 1.— Cumulative function of SB(H α) for DDO 53. Two break points are present. The one at - 20.5 gives the limiting value between the noise and the emission, while the other at - 17.3 divides the spectra between DIG and H II regions.

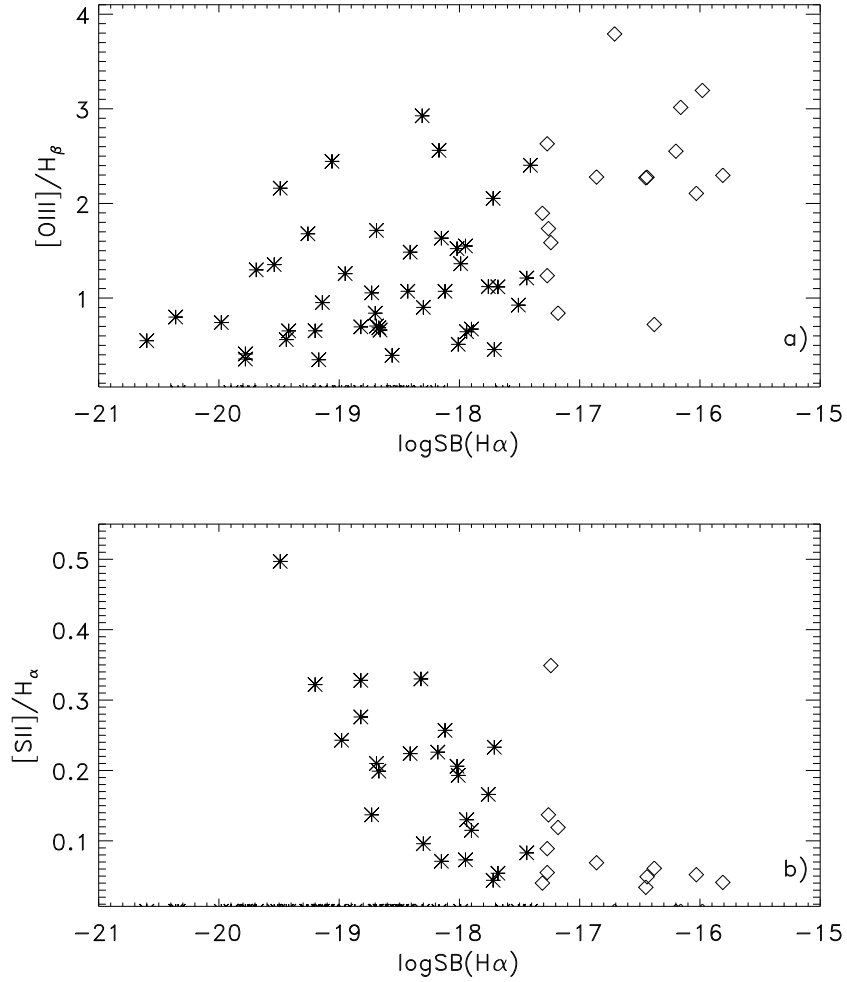


Fig. 2.— Plot of $\log SB(H\alpha)$ vs. $[OIII]/H\beta$ (top) and the $\log SB(H\alpha)$ vs. $[SII]/H\alpha$ (bottom) for DDO 53. The DIG locations are plotted as asterisk, and the H II regions as diamonds (see text for a definition). A smooth transition between the DIG and H II regions is clear from both plots, indicating that our definition of H II regions is correct.

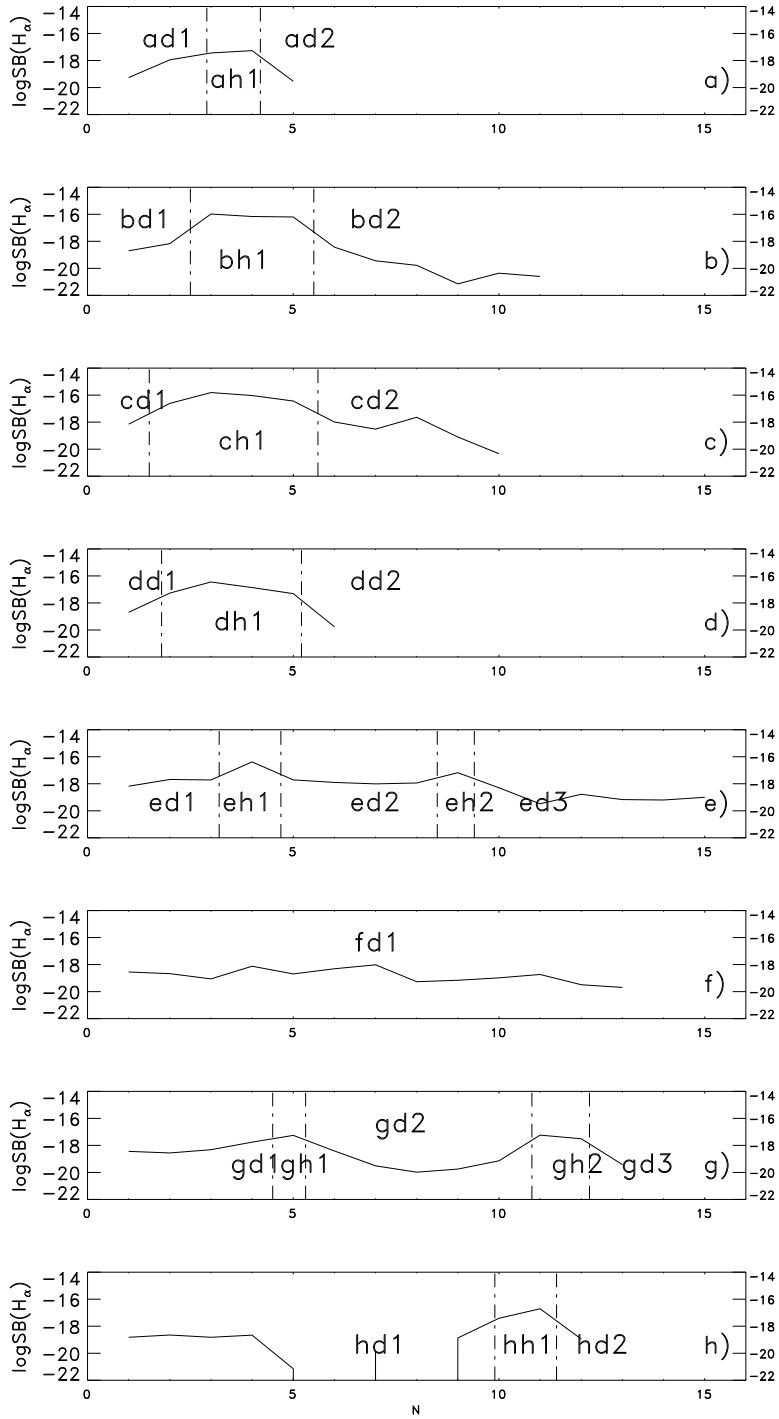


Fig. 3.— SB($H\alpha$) along the slits in DDO 53. Slit a corresponds to the northern part of the galaxy and slit h to the southern. West is to the left. The dot-dashed lines encompass those regions where the flux is higher than 5×10^{-18} ergs s $^{-1}$ cm $^{-2}$ arcsec $^{-2}$.

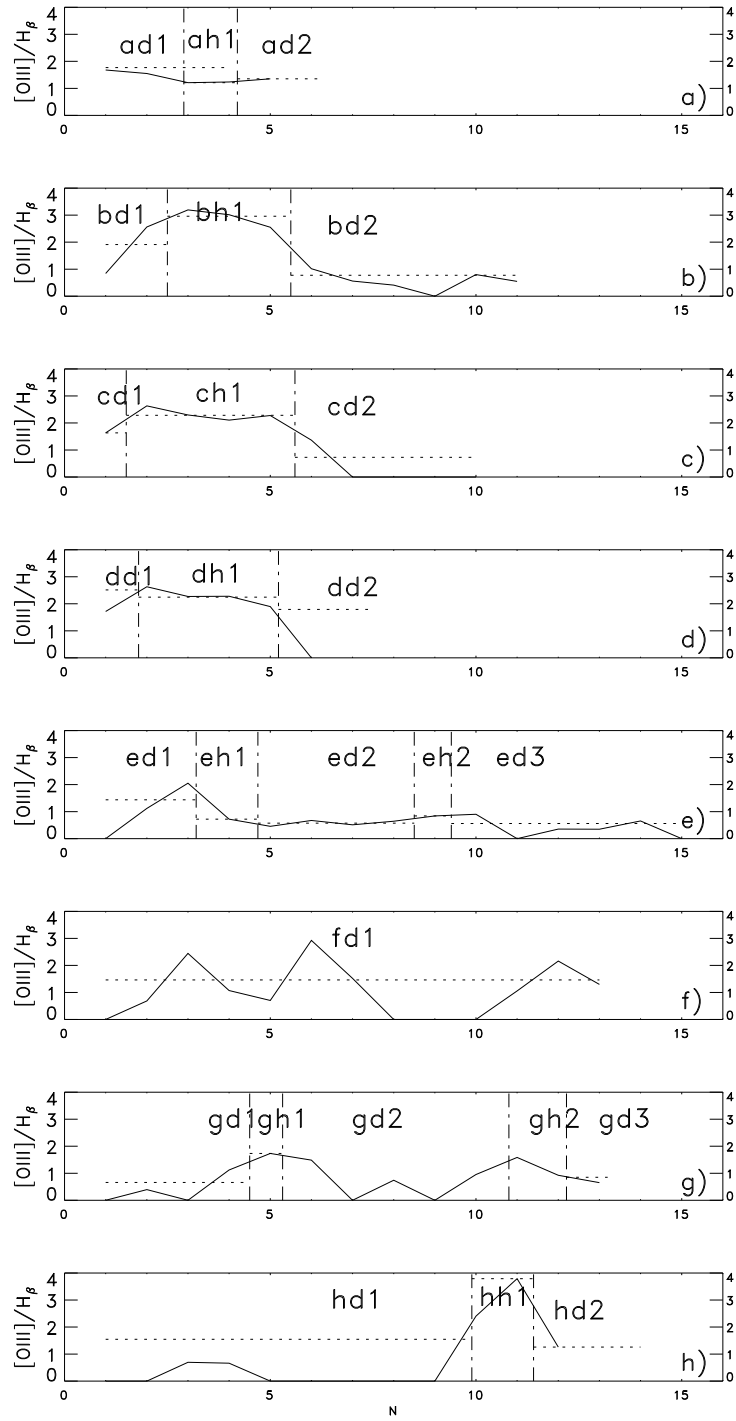


Fig. 4.— $[O III]/H\beta$ along the slits in DDO 53. The symbols and orientation are as in Fig. 3. In addition to those, the dotted lines correspond to the values from the integrated spectra.

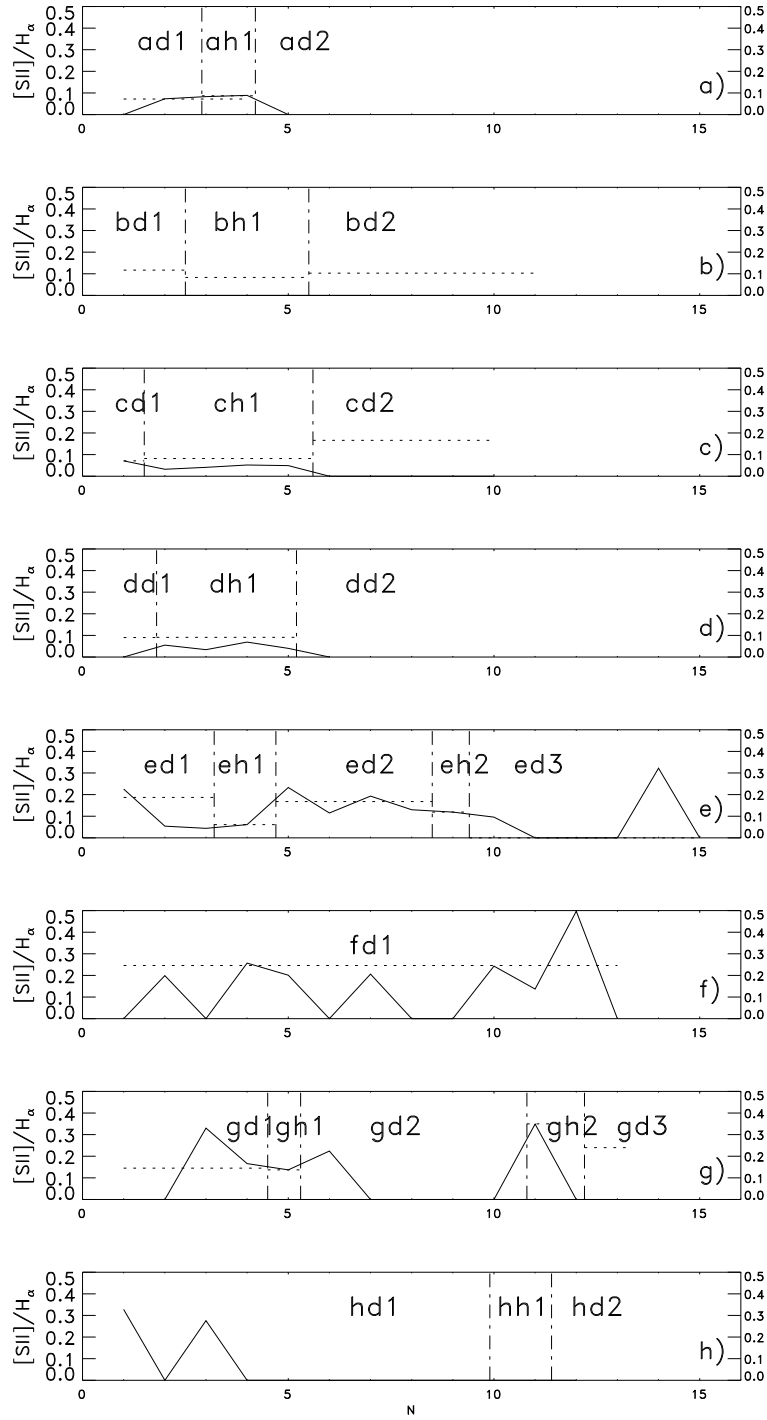


Fig. 5.— $[SII]/H\alpha$ ratio along the slits in DDO 53. The symbols and orientation are as in Fig. 4.

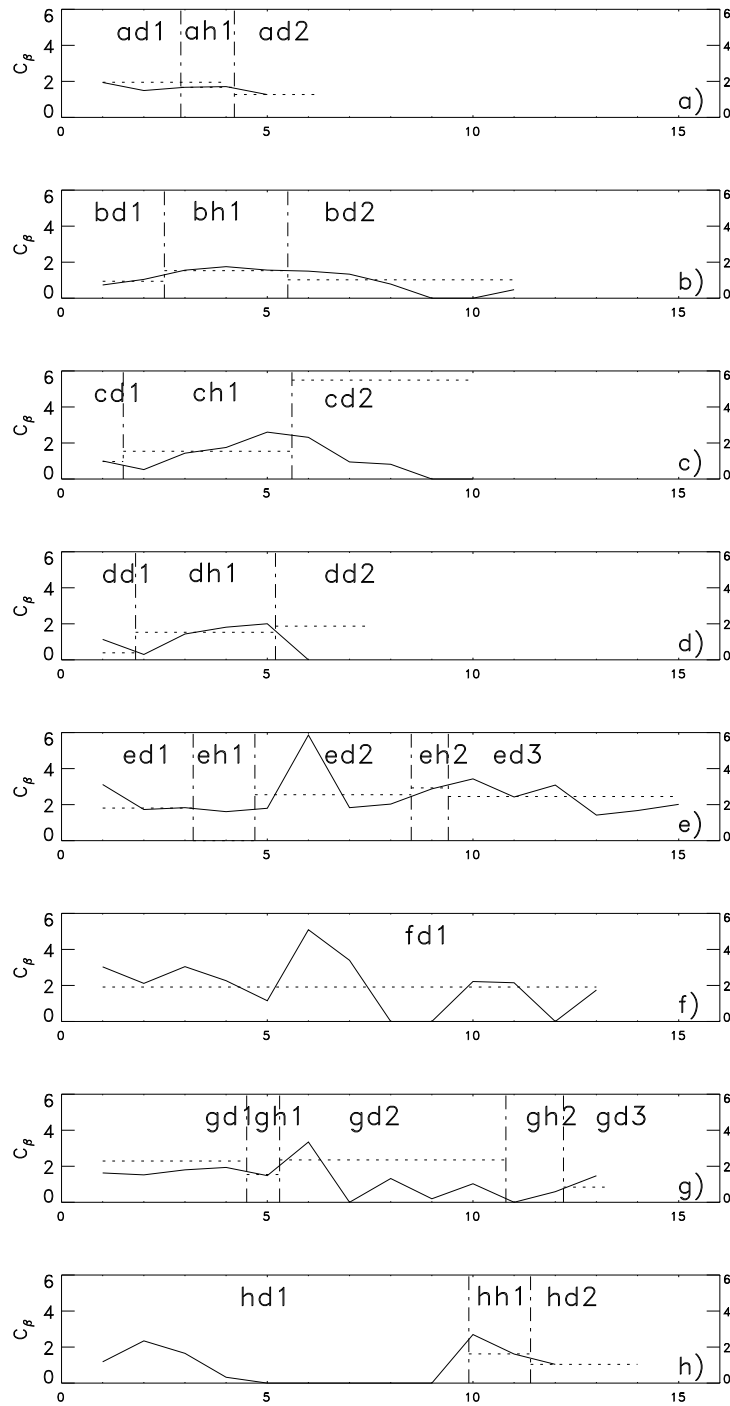


Fig. 6.— Extinction coefficient along the slits in DDO 53. The symbols and orientation are as in Fig. 4.

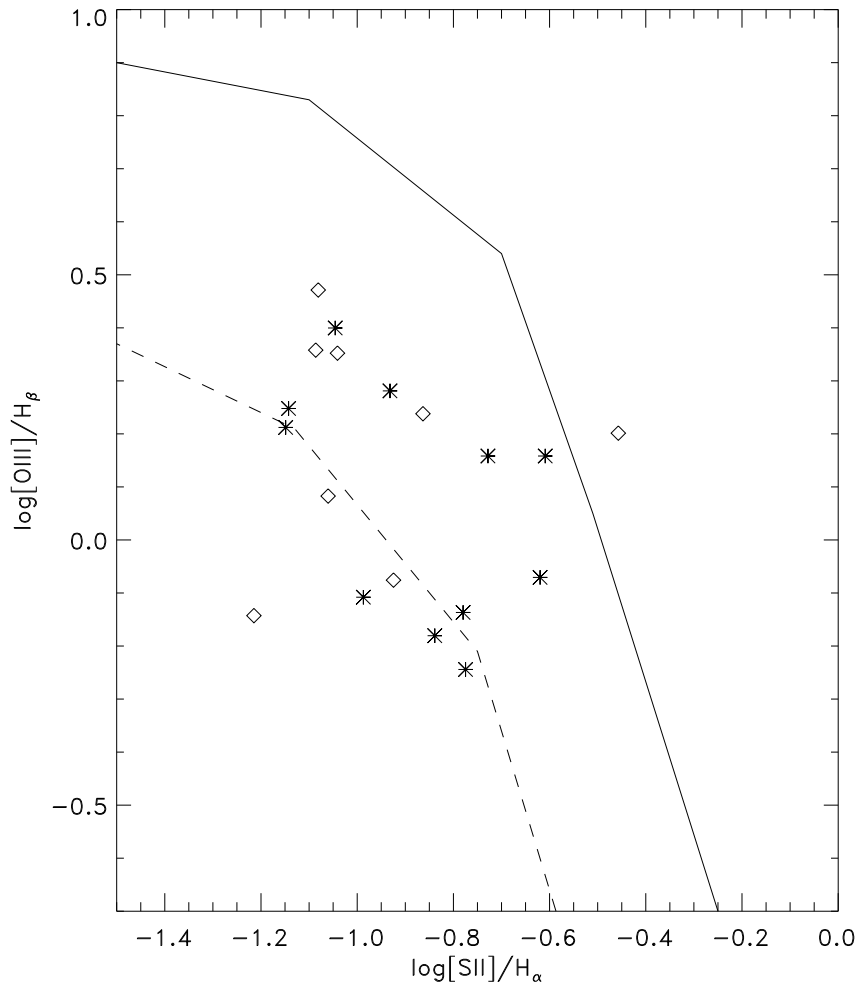


Fig. 7.— $[SII]/H\alpha$ vs. $[OIII]/H\beta$ diagnostic diagram. The diamonds correspond to H II regions, and asterisk to DIG locations. Superimposed are tracks of ionization temperature 50,000 K (*solidline*) and 35,000 K (*dashedline*), from photoionization models at low metallicity from Martin (1997).

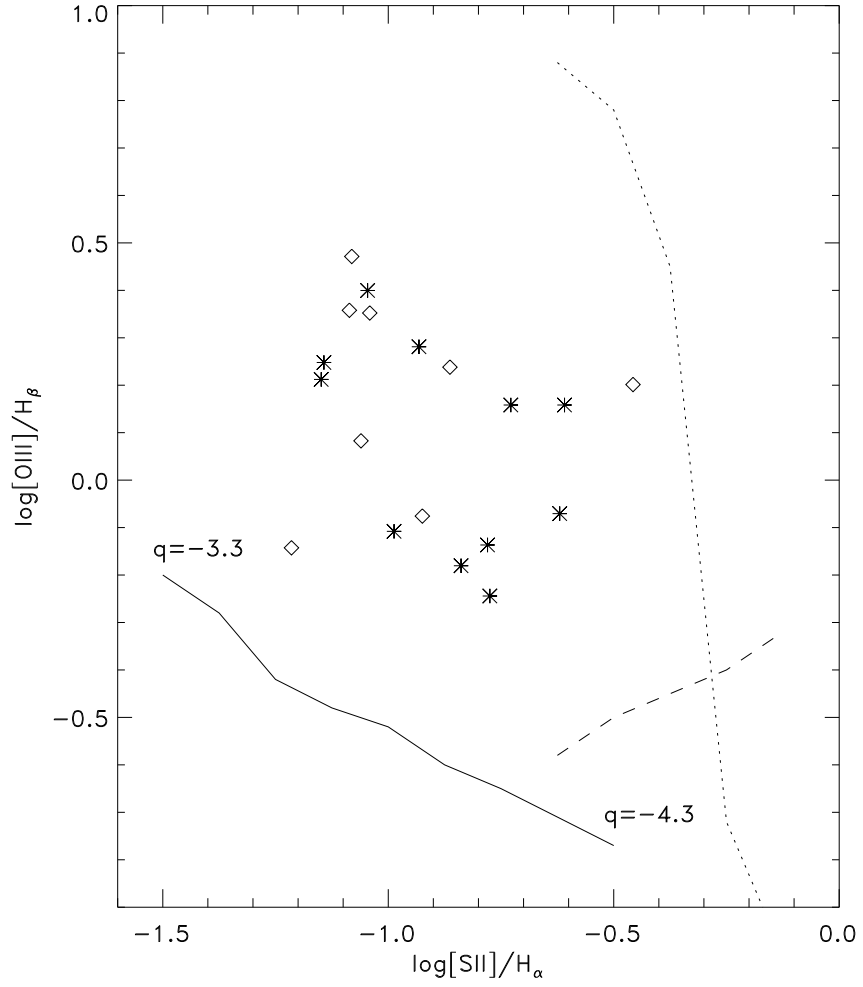


Fig. 8.— $[S\text{II}]/H_\alpha$ vs. $[O\text{III}]/H_\beta$ diagnostic diagram. The diamonds correspond to H II regions, and asterisk to DIG locations. Superimposed are tracks of different models: density-bounded (*solidline*), radiation-bounded (*dottedline*) and turbulent mixing layers (*dashedline*) from Rand (1998).

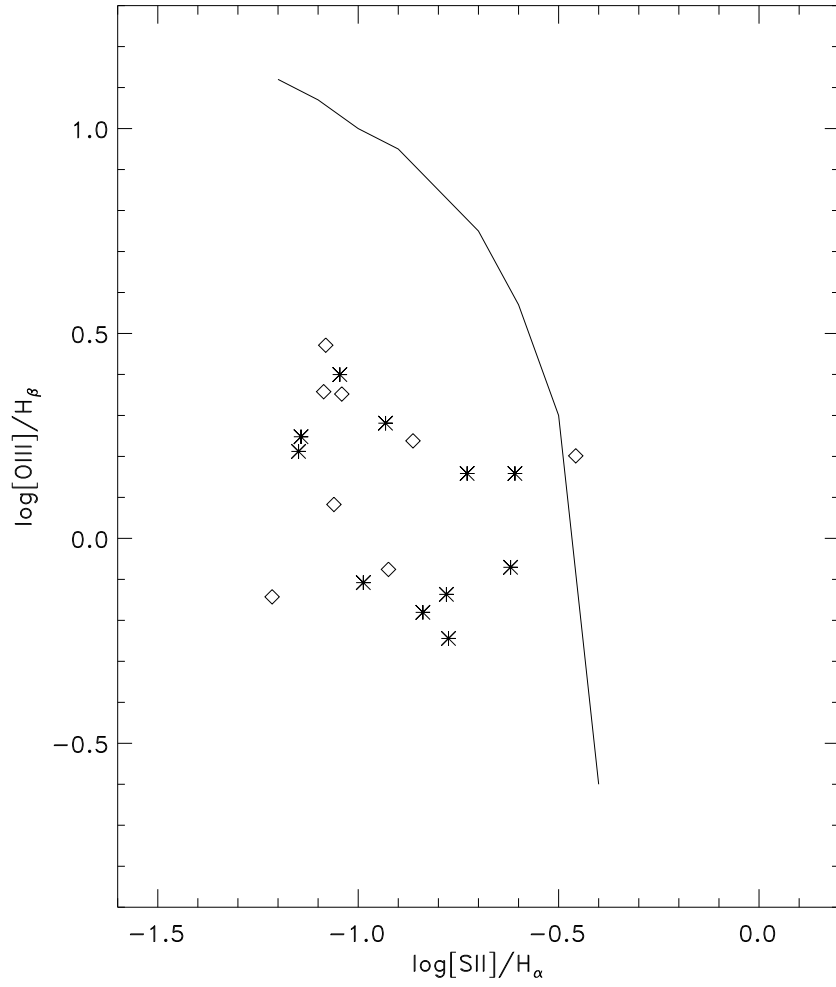


Fig. 9.— $[SII]/H\alpha$ vs. $[OIII]/H\beta$ diagnostic diagram. The diamonds correspond to H II regions, and asterisk to DIG locations. The solid line divides the diagram into the shocked regions (to the left) and the photoionization regions (to the right).

Table 1: Log of the Observations. The slit positions observed are presented in column 1. Column 2 shows the date of observation while the seeing is given in column 3 in arcsecond. The total integration time in minutes is presented in column 4 and the air mass in column 5. Column 6 gives the telescope coordinates for the first slit position for each night while the rest of the positions is given by the number of arcseconds the telescope was moved from the initial position.

Position	Date	Seeing	Int. Time	Air Mas.	Comments
slit a	12032002	1.5''	60 ^m	1.3	08 ^h 34 ^m 66°10'
slit b	12032002	1.5''	85 ^m	1.2	7'' towards the south
slit c	13032002	1.5''	130 ^m	1.2	08 ^h 34 ^m 18 ^s 66°09'51''
slit d	13032002	1.5''	15 ^m	1.2	6'' towards the south
slit e	14032002	2''	70 ^m	1.2	08 ^h 34 ^m 15 ^s 66°09'25''
slit f	14032002	2''	30 ^m	1.2	6'' towards the south
slit g	14032002	2''	30 ^m	1.2	12'' towards the south
slit h	14032002	2''	30 ^m	1.3	18'' towards the south

Table 2: Total uncertainties in the lines ratios studied for each slit position for the DIG locations (at the top) and the H II regions. Three different terms have been considered: the uncertainty in the continuum, the uncertainty due to the reduction and calibration procedure, and the uncertainty due to the extinction correction. For the blended lines an extra term has been considered. Those line ratios not detected at one slit location are marked with -.

Slit	[O III]/H β	[O III]/H α	[N II]/H α	[S II]/H α
slit a	4%	3%	12%	-
slit b	3%	4%	12%	12%
slit c	2%	2%	12%	12%
slit d	2%	2%	-	12%
slit e	3%	3%	24%	13%
slit f	5%	5%	12%	13%
slit g	4%	3%	12%	14%
slit h	5%	5%	15%	16%
slit a	2%	2%	10%	-
slit b	2%	2%	10%	10%
slit c	2%	2%	17%	10%
slit d	2%	2%	14%	10%
slit e	2%	2%	14%	11 %
slit f	-	-	-	-
slit g	2%	2%	10%	10%
slit h	2%	2%	10%	-

Table 3: Extinction-corrected line ratios of the integrated spectra for DDO 53. Column 1 shows the location, where the first character is the slits position from Table 1 and the second is “h” for H II region and “d” for DIG location. The third character is 1 for the first (or only) location in the slit and higher for additional locations. Columns 2, 3 and 4 show the [O III]/H β ratio, the [O III]/H α ratio and the [S II]/H α ratio when detected. Finally, column 5 shows the extinction coefficient in the recombination line H α and the S/N ratio in H α is given in column 6.

Location	[O III]/H β	[O III]/H α	[S II]/H α	C β	S/N(H α)
240 ad1	1.77 \pm 0.07	0.62 \pm 0.03	0.072 \pm 0.01	2.00 \pm 0.06	21
ah1	1.21 \pm 0.05	0.42 \pm 0.03	0.087 \pm 0.007	1.72 \pm 0.07	61
ad2	1.35 \pm 0.2	-	-	-	3
bd1	1.91 \pm 0.06	0.67 \pm 0.03	0.117 \pm 0.007	0.99 \pm 0.08	18
bh1	2.96 \pm 0.05	1.03 \pm 0.02	0.083 \pm 0.007	1.58 \pm 0.06	188
bd2	0.78 \pm 0.09	0.27 \pm 0.03	0.103 \pm 0.02	1.07 \pm 0.07	10
cd1	1.63 \pm 0.2	-	0.071 \pm 0.01	-	13
ch1	2.28 \pm 0.09	0.80 \pm 0.03	0.082 \pm 0.007	1.59 \pm 0.06	55
cd2	0.73 \pm 0.1	0.25 \pm 0.04	0.166 \pm 0.03	5.54 \pm 0.8	4
dd1	2.51 \pm 0.08	0.88 \pm 0.03	0.090 \pm 0.007	0.44 \pm 0.03	18
dh1	2.25 \pm 0.08	0.79 \pm 0.03	0.091 \pm 0.006	1.58 \pm 0.06	81
dd2	1.79 \pm 0.2	0.63 \pm 0.07	-	1.92 \pm 0.1	9
ed1	1.44 \pm 0.2	0.50 \pm 0.07	0.187 \pm 0.03	1.86 \pm 0.3	3
eh1	0.72 \pm 0.02	-	0.061 \pm 0.005	-	20
ed2	0.57 \pm 0.06	0.20 \pm 0.02	0.168 \pm 0.02	2.55 \pm 0.3	8
eh2	0.84 \pm 0.03	0.29 \pm 0.01	0.119 \pm 0.02	2.93 \pm 0.1	26
ed3	0.56 \pm 0.07	0.20 \pm 0.02	-	2.45 \pm 0.3	9
fd1	1.44 \pm 0.2	0.51 \pm 0.07	0.246 \pm 0.04	1.96 \pm 0.3	4
gd1	0.66 \pm 0.08	0.23 \pm 0.03	0.145 \pm 0.03	2.29 \pm 0.1	10
gh1	1.73 \pm 0.06	0.61 \pm 0.02	0.137 \pm 0.02	1.54 \pm 0.03	29
gd2	0.94 \pm 0.1	0.33 \pm 0.04	-	2.35 \pm 0.3	13
gh2	1.59 \pm 0.2	-	0.349 \pm 0.05	-	15
gd3	0.85 \pm 0.1	0.30 \pm 0.04	0.24 \pm 0.05	0.84 \pm 0.04	10
hd1	1.55 \pm 0.2	0.54 \pm 0.08	-	2.71 \pm 0.4	3
hh1	3.79 \pm 0.1	-	-	-	31
hd2	1.26 \pm 0.2	-	-	-	3

Table 4: Photon leakage (in %) and ionization temperatures for the integrated spectra for DDO 53 based on the line ratios. The locations are named as in Table 3. The second and third columns correspond to the data from the excitation and the fourth and fifth are based on the [S II]/H α ratio, when detected.

Location	T_{ion} K	Leakage [O III] (%)	T_{ion} K	Leakage [S II](%)
ad1	38,000-50,000	30-90 %	30,000-34,000	30-35 %
ad2	38,000-41,000	40-70 %	-	- %
bd1	41,000-50,000	50-80 %	30,000-36,000	30-38 %
bd2	38,000	52 %	30,000-36,000	30-40 %
cd1	38,000-47,000	35-80 %	30,000-34,000	30-35 %
cd2	38,000	60 %	30,000-38,000	30-42 %
dd1	41,000-50,000	42-65 %	30,000-34,000	30-35 %
dd2	41,000-50,000	50-90 %	-	-
ed1	38,000-44,000	38-90 %	30,000-40,000	30-45 %
ed2	38,000	72 %	30,000-38,000	30-42 %
ed3	38,000	75 %	-	-
fd1	38,000-41,000	38-85 %	30,000-40,000	35-50/70-80 %
gd1	38,000	62 %	30,000-38,000	30-42 %
gd2	38,000-41,000	50-90 %	-	-
gd3	38,000	55 %	30,000-40,000	35-50/70-80 %
hd1	38,000-44,000	35-85 %	-	-
hd2	38,000-41,000	42-68 %	-	-

Table 5: Line intensities, normalized to $H\beta$, detected inside two of the $H\text{ II}$ regions in DDO 53. The values are absorption and extinction corrected.

Line	region No 10	region No 13
$[\text{O II}]\lambda 3727$	4.6 ± 0.5	0.21 ± 0.01
$[\text{Ne III}]\lambda 3970$	0.20 ± 0.01	0.048 ± 0.001
$H\delta\ \lambda 4102$	0.20 ± 0.01	0.142 ± 0.003
$H\gamma\ \lambda 4340$	0.47 ± 0.01	0.40 ± 0.01
$[\text{O III}]\lambda 4363$	0.056 ± 0.002	0.033 ± 0.002
$\text{He I}\ \lambda 4471$	0.043 ± 0.001	-
$H\beta\ \lambda 4865$	1.00 ± 0.02	1.00 ± 0.02
$[\text{O III}]\lambda 4959$	0.96 ± 0.04	0.78 ± 0.02
$[\text{O III}]\lambda 5007$	2.79 ± 0.09	2.27 ± 0.05
$[\text{N I}]\lambda 5198$	0.021 ± 0.001	0.044 ± 0.001
$\text{He I}\ \lambda 5875$	0.08 ± 0.01	0.01 ± 0.007
$H\alpha\ \lambda\ 6568$	2.86 ± 0.06	2.86 ± 0.06
$[\text{N II}]\lambda 6583$	0.026 ± 0.004	-
$\text{He I}\ \lambda 6678$	0.029 ± 0.001	0.030 ± 0.01
$[\text{S II}]\lambda 6617$	0.136 ± 0.003	0.165 ± 0.004
$[\text{S II}]\lambda 6631$	0.100 ± 0.002	0.119 ± 0.003

Table 6: Electron temperatures, Oxygen and Nitrogen abundances as well as Helium abundances of two of the H II regions in DDO 53, determined with the standard method.

Line	region No 10	region No 13
T_e (O^{++})	15214	13258
T_e (O^+)	13650	12281
$12+\log(O/H)$	7.8 ± 0.1	7.91 ± 0.3
$12+\log(N/H)$	5.67 ± 0.2	-
$\log(N/O)$	-2.12 ± 0.2	-
He^+/H^+	0.11 ± 0.01	0.11 ± 0.03

Table 7: Oxygen Abundances of the H II regions in DDO 53. The identification of the H II region according to Strobel et al. (1990) is given in column 1. The oxygen abundances based on the standard method with the electronic temperature are given in column 2 for the only two regions where the [O III] λ 4363Å line was detected. The oxygen abundances determined with the R₂₃ calibrator by Pagel et al. (1979) are shown in column 3 while the abundances determined with the *P* calibrator by Pilyugin (2001) are shown in column 4.

H II region	12+log(O/H)	R ₂₃	P _b
No 9	-	7.53±0.4	7.48±0.3
No 10	7.80±0.1	8.07±0.3	7.95±0.2
No 13	7.91±0.3	7.98±0.5	7.94±0.4
No 5	-	7.33±0.4	7.23±0.3
No 6	-	7.01±0.5	6.76±0.4
No 11	-	7.17±0.4	6.98±0.3
No 8	-	7.82±0.4	7.82±0.4
No 16	-	7.76±0.5	7.76±0.4
No 17	-	8.10±0.4	-